Applied Catalysis B: Environmental 224 (2018) 533–540

Contents lists available at ScienceDirect

Applied Catalysis B: Environmental

journal homepage: www.elsevier.com/locate/apcatb

N-Doped Porous Molybdenum Carbide Nanobelts as Efficient Catalysts for Hydrogen Evolution Reaction

Shengyu Jing[a], Lishang Zhang[a,b], Lin Luo[b,*], Jiajia Lu[b], Shibin Yin[b,*], Pei Kang Shen[b], Panagiotis Tsiakaras[c,d,e,*]

[a] School of Information and Control Engineering, China University of Mining and Technology, Xuzhou 221116, Jiangsu, China.
[b] Guangxi Key Laboratory of Electrochemical Energy Materials, Collaborative Innovation Center of Renewable Energy Materials (CICREM), State Key Laboratory of Processing for Non-ferrous Metal and Featured Materials, Guangxi University, Nanning 530004, China.
[c] Laboratory of Electrochemical Devices based on Solid Oxide Proton Electrolytes, Institute of High Temperature Electrochemistry, Yekaterinburg 620990, Russia.
[d] Laboratory of Materials and Devices for Electrochemical Power Industry, Ural Federal University, 19 Mira Str., Yekaterinburg 620002, Russia.
[e] Laboratory of Alternative Energy Conversion Systems, Department of Mechanical Engineering, School of Engineering, University of Thessaly, Pedion Areos 38834, Greece.

ARTICLE INFO

Keywords:
water splitting
molybdenum carbide
noble-metal-free catalysts
hydrogen evolution reaction

ABSTRACT

Electrochemical water splitting has been highly valued as a clean and sustainable method to produce hydrogen with high purity and large quantity. Platinum (Pt) possesses excellent performance for hydrogen evolution reaction (HER), however, the expensiveness and rareness still restricts its broad application. Here, an environmentally-friendly and template-free method is developed to synthesize N-doped molybdenum carbide in three different forms: nanobelts, nanorods and nanoparticles. During the synthesis, no additional acid or alkali aqueous solution is used and the morphology is controlled by adjusting water content and treatment time. The corresponding physicohemical and electrochemical results display that the nanobelts with porous nanostructure exhibit excellent activity and good stability for HER both in acidic and alkaline electrolytes. In the latter case (1.0 M KOH aqueous solution), nanobelts show a small onset potential value (–52 mV), yield a current density of 10 mA cm^{-2} at a relatively low overpotential (110 mV) and exhibit a low Tafel slope (49.7 mV dec^{-1}). From the obtained results is deduced that this is a facile way to prepare cost-effective molybdenum carbide with high efficiency for hydrogen evolution.

1. Introduction

With the development of the modern society, hydrogen has been increasingly demanded as an alternative energy carrier to replace the exhaustible fossil fuels such as oil and nature gas. More than 95% of the hydrogen production is achieved industrially through methane steam reforming and coal gasification. However, these methods require huge amounts of fuels and emit a huge quantity of hazardous and environmentally harmful gases [1–3].

The evolution of hydrogen through water splitting has attracted increasing attention, which is inherently a high-performance and environmentally friendly method to produce hydrogen with high purity [4]. It is known that the electrolysis of water involves two reactions: the hydrogen evolution reaction (HER) at the anode and the oxygen evolution reaction (OER) at the cathode [5]. During the HER process, protons in the electrolyte are absorbed on the surface of the anode electrode, and then reduced to hydrogen as the voltage applied to the electrode gets higher than HER's overpotential. Therefore, a catalyst with small overpotential is significant for the H_2 evolution, because it can reduce the power consumption for water splitting.

It is also well known that, platinum (Pt)-based materials are the most efficient catalysts for the reaction of hydrogen evolution both in acid and alkaline solutions [6,7]. However, due to the rareness and the expensiveness of Pt, it is necessary to develop low-Pt or non-Pt catalysts [8,9]. Non-precious metal (NPM) catalysts that usually composed with earth-abundant elements, such as Fe, Co, Ni and so on, displayed almost comparable catalytic activity with Pt [10]. Meanwhile, some of them also exhibited good stability during the accelerated durability tests, providing a cheaper alternative for hydrogen production in large scale.

The NPM catalysts, such as metal sulfides [11–13], selenides [14], carbides [15,16], nitrides [17,18], phosphides [19–21], complexes [22] or even semi-metal/conductor [23,24] have been widely investigated.

Among the four existed phases of molybdenum carbides (α-MoC_{1-x}, η-MoC, γ-MoC, and β-Mo_2C), β-Mo_2C is considered as the most active configuration [25]; it exhibits higher HER activity and good stability both in acid and alkaline solutions. The reason may be ascribed to its

* Corresponding authors.
E-mail addresses: luolin@gxu.edu.cn (L. Luo), lyinshibin@gxu.edu.cn (S. Yin), tsiak@uth.gr (P. Tsiakaras).

http://dx.doi.org/10.1016/j.apcatb.2017.10.025
Received 28 August 2017; Received in revised form 5 October 2017; Accepted 11 October 2017
Available online 13 October 2017

high similarity with Pt-based catalysts; specifically, the incorporation of carbon atoms into the lattice interstitials of molybdenum affords them with *d*-band electronic structures that are similar to Pt benchmark [26]. Many studies demonstrated that the HER activity of Mo_2C could be improved by constructing proper morphologies, such as nanowires and nanoparticles, owing to the enhanced exposure of active sites on the surface [27,28]. Another improvement strategy concerns with the introduction of other elements, such as nitrogen [17], phosphorus [20], sulfur [29] and boron [30]; these elements may tune the electronic states of Mo and make the active sites distribute in a desirable way. Furthermore, the introduction of heteroatoms might also regulate the electronic arrangements of carbon skeleton, and consequently increase the corresponding catalytic activity for HER [31]. Liu et al. indicated that the metal carbides embedded in nitrogen-doped carbon exhibited high HER activities; this is mainly due to the most favorable H^+ absorption/desorption property and the synergistic effect between Mo_2C and the N-doped hybrid catalysts [32,33].

However, during the high temperature reduction, an aggregation and/or an excessive growth of Mo_2C particles is occurred, decreasing the specific area and thus lessen the catalytic activity for water splitting; nevertheless, it could be restrained by uniform distribution of Mo_2C particles in catalysts. Lou [34] and Chen [35] et al. employed a template method to fabricate Mo_2C catalysts for hydrogen evolution. The prepared materials showed a uniformly distributed Mo_2C-CNT structure and alkaline and acid environments were required during the synthesis processing. Meanwhile, some Mo_2C nanomaterials were obtained by organic polymerization strategy. Li et al. [36] synthesized Mo_2C nanoparticles uniformly dispersed on hierarchical carbon microflowers, however, ammonium hydroxide was employed as alkaline aqueous solution that releases irritating smell. Gao et al. [37] prepared Mo_2C nanowires doped with Co, during which 1.0 M HCl aqueous solution was needed.

In summary, up to date, the above reported methods for preparing Mo_2C usually involve complex and/or relatively dangerous procedures, expensive and/or environmentally unfriendly precursors or templates, which will hinder their practical applications [38].

In this work, a cost-efficient and environmentally-friendly method to synthesize N-doped porous molybdenum carbide (β-Mo_2C) nanomaterials without template is reported. During the synthesis, no additional acid or alkali aqueous solution is used, while the morphology can be controlled by adjusting the water content and treatment time. Three different morphologies (nanobelts, nanorods and nanoparticles) of molybdenum carbide (Mo_2C) were prepared, and the corresponding physicochemical and electrochemical characterizations were investigated and thoroughly discussed. The results indicated that the as prepared nanobelts offer a cheaper solution for high catalytic activity and good stability of hydrogen evolution reaction.

2. Experimental

2.1. Preparation

Melamine ($C_3N_3(NH_2)_3$, MA), which has 66.7 wt% of nitrogen, was used as the carbon and nitrogen source. The schematic diagram is shown in Fig. 1a. Step 1 is the *chaining process* of the precursor. Through heating the solution of ammonium molybdate tetrahydrate ($(NH_4)_6Mo_7O_{24}{\cdot}4H_2O$) and ethylene glycol ($(CH_2OH)_2$, EG), ammonia ions are converted to ammonia gas. The remaining hydrogen cations are combined with EG to form protonated EG ($(CH_2OH)_2$-H_2^+, PEG), and then chaining with molybdate ion ($Mo_7O_{24}{}^{6-}$) to form a chain shape. Step 2 is the *substitution and aggregation process*. As the protonated melamine ($(C_3N_3(NH_2)_3$-$H^+_{3/2/1}$, PMA) is added into the above solution, the substitution reaction occurs on PEG and a white precipitation begins to appear.

Meanwhile, the coordination of $Mo_7O_{24}{}^{6-}$ ions with amino groups could form a high density of catalytically active sites in the as-prepared samples [28]. As reported, the octahedric structure of molybdate share two vertexes at the ortho-position, and thus zig-zag chains will interlink each other through the cis-position, leading to the spontaneous arrangement of crystalline structure by means of electrostatic interactions between ions, such as $NH_4{}^+$ and OH^-. Furthermore, the H^+ in PEG could serve this role [39–41]. Given that in this work water acts as a carrier of PMA, redundant protonated and unprotonated amidogen may exist in the substituted chains. The substitution reaction of PMA and the aggregated reaction of the chains could simultaneously occur in presence of water, as illustrated in Fig. 1, therefore the morphologies of the as-prepared samples could be simply controlled by changing the water content.

Typically, nanobelts were prepared as follows: 5.0 mmol $(NH_4)_6Mo_7O_{24}{\cdot}4H_2O$ was dissolved in 20.0 ml ethylene glycol and stirred in oil bath at 80 °C for 18 h. Another solution with 32.0 mmol melamine, 20.0 ml ethylene glycol and 8.0 ml deionized water that prepared at the same condition was added into above solution. After stirring for 1 h, the white precipitation was collected by centrifugation and washed with ethanol. Finally, the resulting powders were heated in a tube furnace at 800 °C under a flow of H_2/Ar (5% H_2) for 2 h with a heating rate of 5 °C min^{-1}. Nanorods and nanoparticles were synthetized by the same way but 15.0 ml and 22.0 ml water was involved, respectively.

2.2. Characterization

X-ray powder diffraction (XRD) measurements were carried out using a SmartLab X-ray diffractometer (Rigaku Corp., Japan) equipped with Cu-Ka radiation ($\lambda = 0.15406$ nm) source. The data was collected at 40 kV and 30 mA with 2θ angular regions between 10° and 90°, with a scan rate of 5° min^{-1}. X-ray photoelectron spectroscopy (XPS) spectra were recorded on a spectrometer ESCALab 250Xi (ThermoFisher Scientific, USA) with an Al X-ray source operated at 150 W. Scanning electron microscopy (SEM) measurements were carried out using a FESEM SU8220 (Hitachi Corp., Japan) to get the information of morphology and structure of the as-prepared catalysts. Scanning transmission electron microscopy (STEM) and energy dispersive X-ray spectroscopy (EDX) investigations were carried out using a Titan ETEM G^2 80-300 (FEI Co., USA) at an accelerating voltage of 200 kV to get the information of particle size distribution and the composition of the as-prepared catalysts. Surface area measurements were performed on an ASAP 2460 Brunauer-Emmett-Teller (BET) analyzer (Micromeritics Instrument Ltd., USA).

Electrochemical measurements were obtained through a computer controlled Pine (Pine, USA) three-electrode system electrochemical workstation. Electrochemical impedance spectroscopy (EIS) measurements were performed in the frequency range from 100 KHz to 100 MHz in a Zahner (Zahner IM6e, Germany). A reversible hydrogen electrode (RHE) and graphite rod was used as reference electrode and counter electrode, respectively. A glassy carbon disk (5.0 mm in diameter), coated by catalysts films, was used as working electrode. The catalysts films were prepared as follows: 5.0 mg of catalyst was dispersed in 1.0 mL solution containing 20.0 μL of 5 wt% Nafion solution and 980.0 μL of ethanol. After ultrasonication for about 40 min a homogeneous ink was obtained, then 20.0 μL the as-prepared slurry was dropped on the electrode by using a micropipette, and then dried in air; the calculated catalysts loading was 0.50 mg cm^{-2}. A Pt/C catalyst (20 wt% Pt/C, Johnson Matthey), used as reference material, was prepared by same way, except 10.0 μL slurry was dropped, and the mass loading was 0.25 mg cm^{-2}. After initial stabilization of activities, the linear sweep voltammetry (LSV) curves were recorded with a scan rate of 5 mV s^{-1} in 0.5 M H_2SO_4 and 1.0 M KOH aqueous solution that purged with N_2. For the electrochemical stability tests, a glassy carbon disk, prepared by above method, as working electrode was used. The HER activities of all the as-prepared catalysts were recorded after sweeping 1,000 cycles from 0 to −0.3 V both in acidic and alkaline

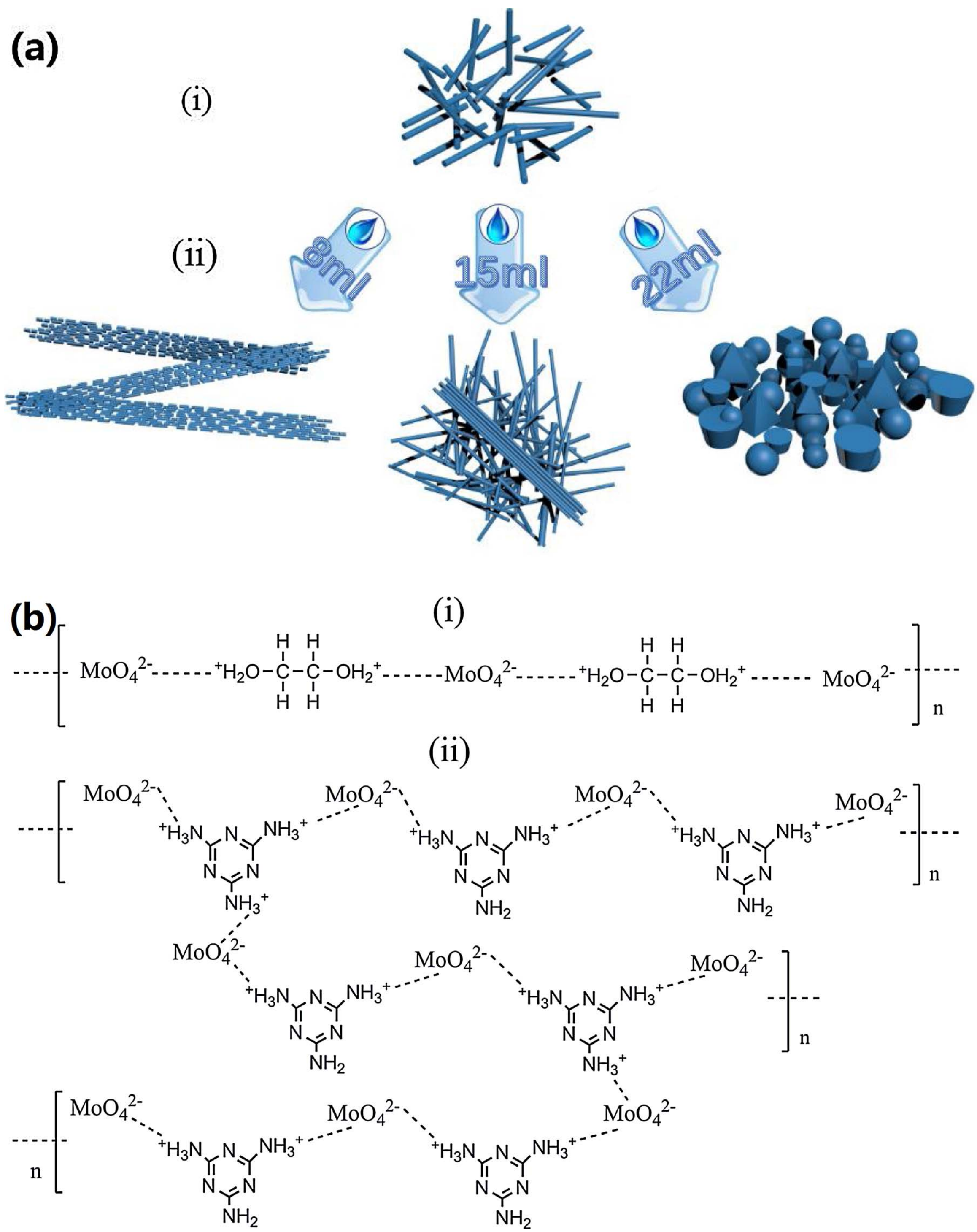

Fig. 1. A brief overview of the synthesis of Mo_2C precursors: (a) schematic illustration and (b) molecular formula.

solutions, and the chronoamperometry curves were obtained by holding the potential at −160 mV and −130 mV in 0.5 M H_2SO_4 and 1.0 M KOH aqueous solutions, respectively. The Tafel slopes were fitted to Tafel equation (η = a + b log(j)); where η (mV) denotes the applied overpotential, j (mA cm^{-2}) the current density and b (mV dec^{-1}) the Tafel slope. Exchange current density (j_0) is calculated by extrapolating the Tafel plots to X-axis according to Tafel equation; j_0 was obtained by assuming η was zero. It should be noted that in this work all measurements were performed at room temperature, all current densities were normalized by geometric area, and all polarization curves were *IR*-corrected.

3. Results and discussion

3.1. Physicochemical characterization

Fig. 2a shows the XRD patterns of the as-prepared Mo_2C nanobelts, nanorods and nanoparticles. The peaks located at 2θ of 34.4°, 37.9°, 39.4°, 52.1°, 61.5°, 69.6°, 72.4° and 74.6° are assigned to (100), (002), (101), (102), (110) (103), (200) and (112) planes of the hexagonal β-Mo_2C (PDF No.#35-0787), which is similar with other reported catalysts that exhibited high HER activities [26,31,32]; similar distribution of peaks indicates that they all are β-Mo_2C. The broad peaks at 26° with

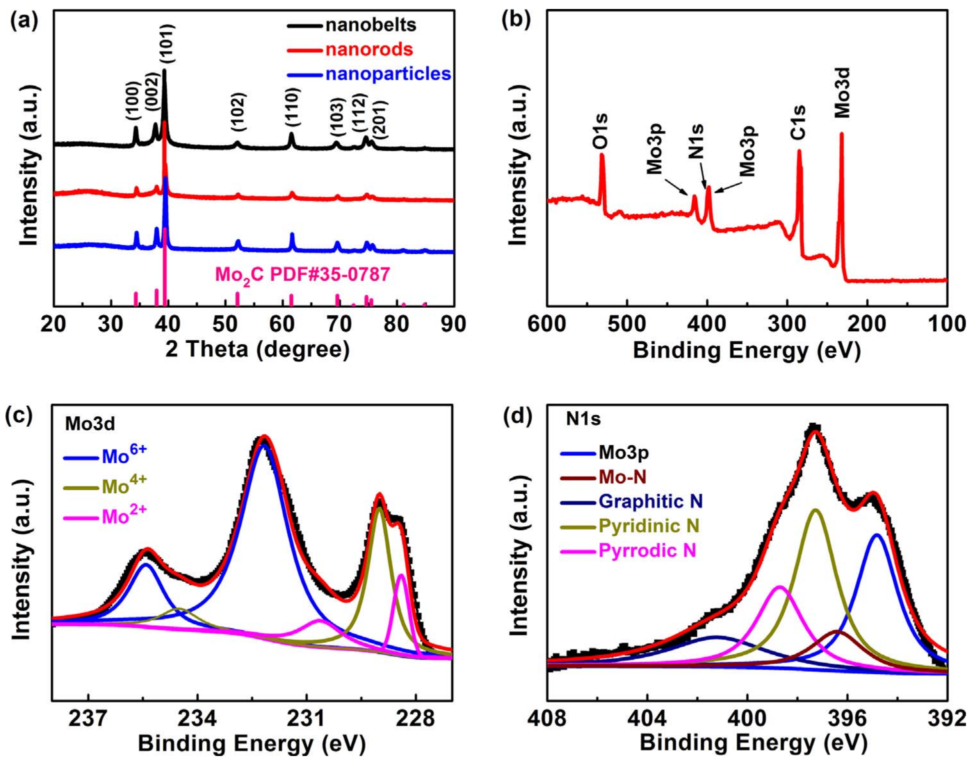

Fig. 2. (a) XRD patterns of Mo_2C nanobelts, nanorods and nanoparticles. (b) XPS summary, (c) Mo3d and (d) N1s of Mo_2C nanobelts.

relatively low intensities are ascribed to carbon derived from melamine.

From the XPS analysis shown in Fig. 2b is deduced that the surface of Mo_2C nanobelts is composed of Mo, N, C, and O. Peak deconvolution of Mo3d verify the existence of Mo_2C (Mo^{2+} at 228.4 and 230.6 eV), MoO_2 (Mo^{4+} at 229 and 230.5 eV), and MoO_3 (Mo^{6+} at 232.2 and 235.5 eV) (Fig. 2c) [25]. The presence of oxides is not surprising and seems to be unavoidable for carbide materials. This may result from the nature of nanosized materials, which are easily oxidized on the surface as they exposed in air [25,36].

As can be seen from Fig. 2d, the N1s XPS spectrum is deconvoluted into three peaks at 396.4, 397.3, 398.7, and 401.3 eV, which correspond to Mo-N, pyridinic-N, pyrrolic-N, and graphitic-N, respectively [36,38,42]. Especially, pyridinic-N exhibits the highest peak in this work and it was proved advantageous for enhancing the catalytic performance of water splitting [43]. Meanwhile, in Fig. S1, it can be seen that all the as-prepared materials have almost similar contents of Mo, C, N, O.

SEM analysis was used to investigate the microscopic morphology of the as-prepared Mo_2C samples. As displayed in Figs. 3a,3b, Mo_2C nanobelts show a porous structure with plentiful pores. During the synthesis process, in presence of 8.0 ml water in the solution, porous belts-like materials were obtained. This is probably due to the following reasons: (i) the substitution reaction may occur slowly and incompletely; (ii) redundant protonated and/or unprotonated amidogen may exist in the substituted chains; (iii) carbonization of precursor during the synthesis process may form interspace between the aggregated chains. As shown in Fig. 1b, this porous structure could provide abundant pores, thus increase the corresponding specific surface area, which could also be favorable for hydrogen evolution reaction by facilitating the transport of electrolyte on the surface. A net like structure of nanorods can be observed in Fig. S2a. Particularly, above the net, clusters made of nanorods can be distinguished. As mentioned above, the formation of clusters and nanorods may occur simultaneously. The surface of the nanorods-net polymerized into clusters under the effect of water during the step 2. Clusters composed with nanorods can be observed from Figs. S2b-S2d, and the unified scale of rods with diameter ranging from approximately 10 to 30 nm can be estimated. Nanoparticles with size from 150 to 500 nm can be seen in Figs. S2i,S2j. Using 22.0 ml water during the synthesis, nanoparticles were obtained *via* drastic substitution and aggregation reaction. Therefore, the amount of water used during the synthesis procedure plays a significant role in altering the corresponding morphology.

The high-angle annular dark-field (HAADF) and EDX technologies were further employed to characterize the elements distribution of the as-prepared materials. Fig. 3e, Fig. S2 g, and Fig. S2m display the HAADF images of nanobelts, nanorods, and nanoparticles, while in Fig. 3f, Fig. S2 h and Fig. S2n are reported the corresponding EDX images. From Fig. S2n, it is obvious that in all Mo_2C samples a uniform distribution of Mo, C, and N elements is achieved. Specially, constituent elements in all samples possess a correlated spatial distribution. The coupling conjugation structure between Mo and C could downshift the *d*-band center of molybdenum by inducing charge transfers from molybdenum to carbon, thus achieving a relatively moderate Mo-H bond strength for enhanced H desorption [44].

The uniform distribution was further proved by the aid of high-resolution TEM (HRTEM). As it can be seen from Fig. 3d, the lattice fringes with interplanar distance of 0.228 and 0.261 nm are clearly displayed. These lattice spacings correspond to the (101) and (100) crystal faces of the Mo_2C materials. The most prominent crystal planes of (101) could also be seen in the HRTEM images of nanorods (Figs. S2e,S2f) and nanoparticles (Fig. S2l).

A sample without employing EG was also prepared in order to prove the vital role of EG. As it can be seen from Fig. S3a, the sample without employing EG shows a bulky morphology with big particles. This may be attributed to the drastic reaction between protonated melamine and molybdate ion in aqueous environment. In step 1, the effect of the treatment time was further investigated. Samples treated for 6 and 12 h in Step 1 were also prepared. As displayed in Fig. S3b, for the sample with 8.0 ml water and treated for 6 h in step 1, the surface is covered with variable lump, while the sample treated for 12 h exhibits single chain and aggregated chains (Figs. S3c,S3d). Similarly, sample synthesized using 15 ml water and treated for 6 h contains fewer rods (Fig. S3e); while as seen in Fig. S3f, for the sample treated in step 1 for 12 h more nanorods are observed. This indicates that the combination of

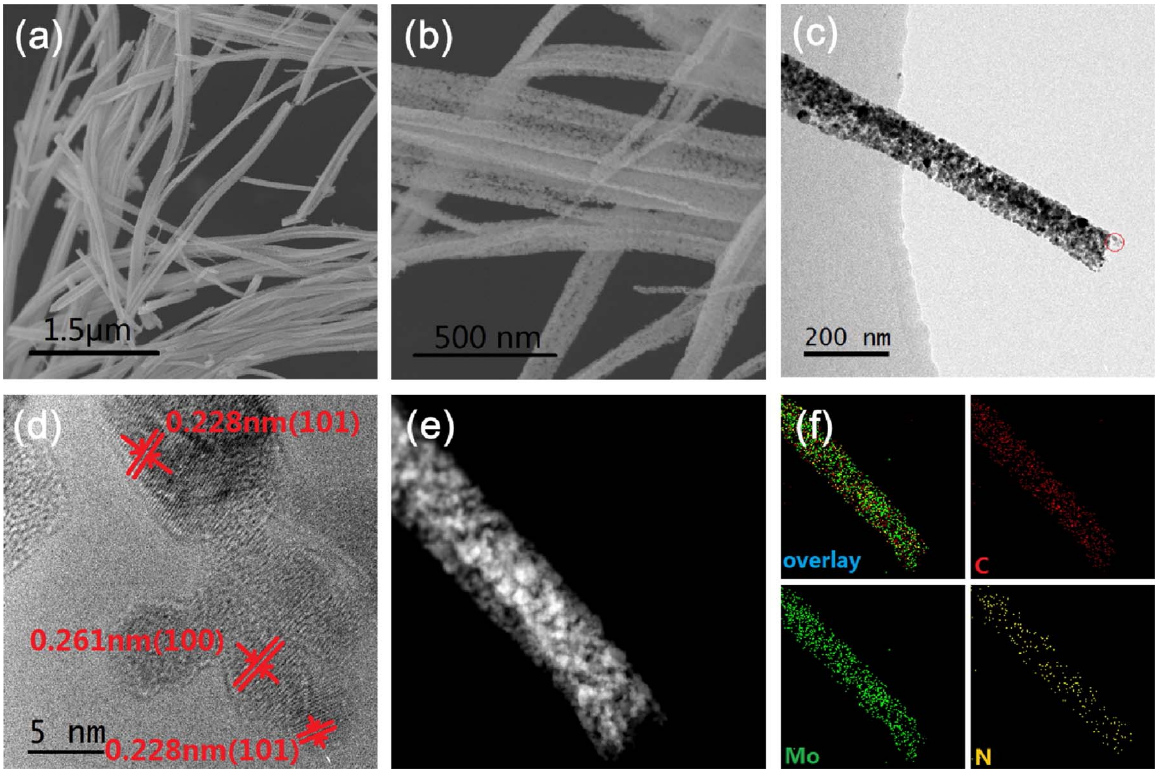

Fig. 3. (a) (b) SEM, (c) TEM, (d) HRTEM (red circle in TEM), (e) HAADF and (f) elemental mapping images of Mo_2C nanobelts.

PEG with molybdate ion may occur through a sluggish reaction and the chain shape could only be obtained after treated long enough. These results, especially single chain and aggregated chains (in Figs. S3c,S3d), could be evidences to prove the substitution and aggregation strategy, as aforementioned.

As shown in Fig. S4 and S5, the SEM, TEM pictures of precursors indicate that the morphologies of Mo_2C samples are in accordance with the precursors, respectively. The EDS images further confirm the composition that the precursors possess a uniform distribution of Mo, C and N elements, O element could be derived from the molybdate in the chains.

3.2. Electrochemical characterization

The as-prepared β-Mo_2C nanomaterials were evaluated as catalysts for HER both in 1.0 M KOH and 0.5 M H_2SO_4 with a scan rate of 5 mV s^{-1}. For comparison reasons, commercial 20 wt% Pt/C was also assessed. As shown in Figs. 4a,4b, the commercial Pt/C displays the highest catalytic activity for water splitting and with an onset potential near to zero. Notably, the current density measured over nanobelts starts with a small onset potential of −52 mV in alkaline and −80 mV in acid solution. These values are smaller than that of β-Mo_2C in the form of nanorods and nanoparticles. The cathodic current density increases rapidly with more negative potentials, which means that the as-prepared nanobelts possess high catalytic activity and good Tafel slopes for water splitting. It is known that, the overpotential at a current density of 10 mA cm^{-2} is another important parameter for water splitting, because 10 ~ 20 mA cm^{-2} is usually operated on solar-light-coupled HER apparatuses under standard conditions [45]. To achieve this current density value, nanorods demand overpotentials of 156 mV and 180 mV, nanoparticles require 171 mV and 189 mV, in 1.0 M KOH and 0.5 M H_2SO_4 aqueous solution, respectively. On the other hand, nanobelts material requires 110 mV and 140 mV of overpotential in alkaline and acid conditions respectively; smaller than those required from nanorods and nanoparticles, indicating a better catalytic activity of nanobelts than nanorods and nanoparticles. As can be seen from Figs. 4c,4d, the fitted lines of Tafel plots yield for nanobelts slopes of approximately 49.7 and 51.3 mV dec^{-1} in 1.0 M KOH and 0.5 M H_2SO_4 aqueous solutions, respectively.

These values are smaller than those obtained for nanorods (of 66.2, 65.5 mV dec^{-1}) and for nanoparticles (of 60, 60.6 mV dec^{-1}) in alkaline and acidic electrolyte, respectively; the values are comparable with that reported in literature recently (Table 1). The small Tafel slopes suggest that the reaction of hydrogen evolution on Mo_2C nanomaterials might be mainly based on the Volmer–Heyrovsky mechanism; in theory Tafel slope is 30 mV dec^{-1}, Heyrovsky slope is 40 mV dec^{-1} and Volmer slope is 120 mV dec^{-1} [27,46].

Commonly, the acidic solution should be favorable for water splitting due to the enough H^+ in the solution able to react with catalysts. However, in this work, the higher HER activity of the three Mo_2C morphologies is observed in alkaline solution. Fact that is consistent with literature data (Table 1), and might be related to the different reaction mechanisms and reaction species involved in the different electrolytes [34,47]. In acid conditions, the HER proceeds *via* the following three different reaction pathways [46,48]:

$$H_3O^+ + e^- + \text{catalyst} \rightarrow \text{catalyst-H} + H_2O \text{ (Volmer-reaction)} \quad (1)$$

$$H_3O^+ + e^- + \text{catalyst-H} \rightarrow \text{catalyst} + H_2 + H_2O \text{ (Heyrovsky-reaction)} \quad (2)$$

$$\text{Catalyst-H} + \text{catalyst-H} \rightarrow 2{*}\text{catalysts} + H_2 \text{ (Tafel-reaction)} \quad (3)$$

In alkaline conditions, there are also three different pathways [46,48]:

$$H_2O + e^- + \text{catalyst} \rightarrow \text{catalyst-H} + OH^- \text{ (Volmer-reaction)} \quad (4)$$

$$H_2O + e^- + \text{catalyst-H} \rightarrow \text{catalyst} + H_2 + OH^- \text{ (Heyrovsky-reaction)} \quad (5)$$

$$\text{Catalyst-H} + \text{catalyst-H} \rightarrow 2{*}\text{catalyst} + H_2 \text{ (Tafel-reaction)} \quad (6)$$

Moreover, the Mo_2C nanobelts show relatively high exchange current density (j_0) of 0.056 mA cm^{-2} in 1.0 M KOH and 0.021 mA cm^{-2}

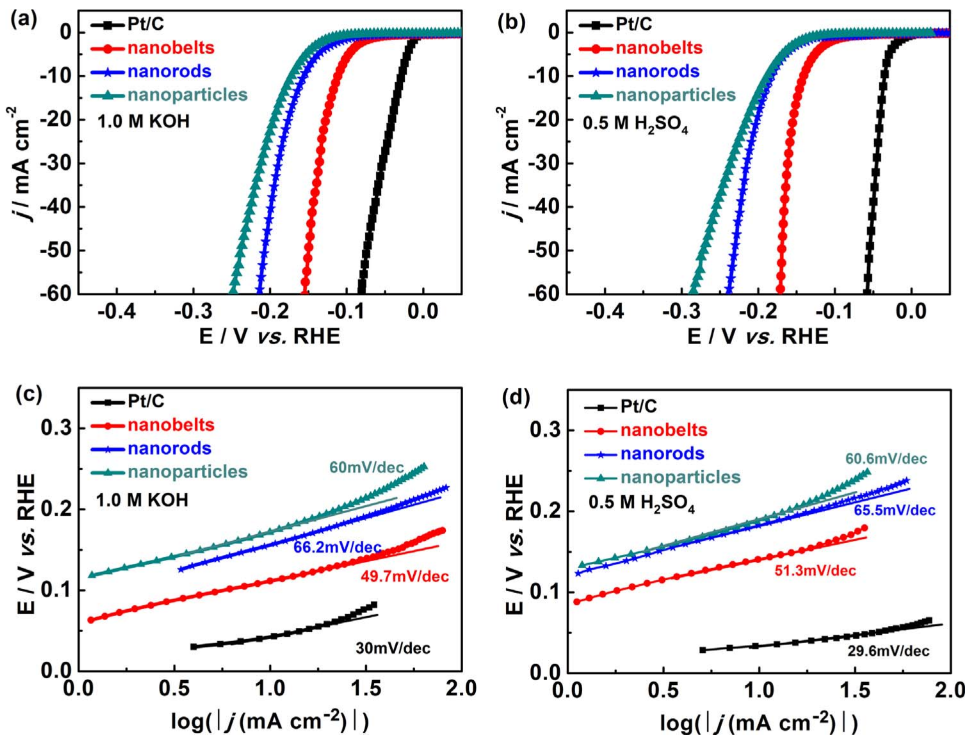

Fig. 4. Electrochemical measurements of Mo_2C materials (different morphologies) for hydrogen evolution. (a) and (b) polarization curves, (c) and (d) the corresponding Tafel plots of Mo_2C and Pt/C benchmark in 1.0 M KOH and 0.5 M H_2SO_4 aqueous solution.

Table 1
Comparison of HER activities for Mo_2C nanobelts with literatures recently reported.

Catalyst	Electrolyte	Overpotential at 10 mA cm^{-2} (mV)	Tafel slope (mV/dec)	Exchange current density (j_0/mAcm^{-2})	Ref.
Mo_2C@N-CNFs	1.0 M KOH	/	/	/	[26]
	0.5 M H_2SO_4	192	70	0.0473	
Mo_2C nano-octahedra	1.0 M KOH	151	59	/	[27]
	0.5 M H_2SO_4	142	53	0.023	
Mo_2C@NC	1.0 M KOH	60	/	/	[32]
	0.5 M H_2SO_4	124	60	0.096	
Mo_2C nanotubes	1.0 M KOH	112	55	0.087	[34]
	0.5 M H_2SO_4	172	62	0.017	
Mo_2CNCNTs	1.0 M KOH	/	/	/	[35]
	0.5 M H_2SO_4	147	71	0.115	
Mo_2C/CNT	1.0 M KOH	100	65	/	[36]
	0.5 M H_2SO_4	144	55	/	
MoC-Mo_2C-31.4	1.0 M KOH	120	42	0.013	[41]
	0.5 M H_2SO_4	126	43	0.011	
N, P/Mo_2C@C	1.0 M KOH	47	71	2.042	[49]
	0.5 M H_2SO_4	141	56	0.029	
M-Mo_2C	1.0 M KOH	128	56	0.0409	[50]
	0.5 M H_2SO_4	135	58	0.0631	
Mo_2C-GNR	1.0 M KOH	121	54	/	[51]
	0.5 M H_2SO_4	152	65	/	
Mo_2C nanobelts	1.0 M KOH	110	49.7	0.056	This work
	0.5 M H_2SO_4	140	51.3	0.021	

in 0.5 M H_2SO_4 aqueous solution, which is also comparable to that recently reported in literatures (Table 1).

To gain further insight into the nature of catalytic activity, electrochemical impedance spectroscopy (EIS) tests were performed. Figs. 5a,b display the obtained Nyquist plots over the as-prepared materials. For clarity the magnified Nyquist plots in high frequency region are presented (insets of the pictures). Compared with the Nyquist plots of Mo_2C nanorods and nanoparticles, Mo_2C nanobelts exhibit a much bigger semicircle. The reason may derive from their discontinuous structure. Remarkably, the Nyquist plot of nanobelts exhibit a semicircle and a line, indicating that the corresponding equivalent circuit is characterized by two time constants, as fitted from the experimental data (Fig. S6). The semicircle at high frequencies is related to the porous property of the electrode's surface, whereas the line with potential-dependent properties at low frequencies is attributed to the kinetics of the HER process [52,53]. The resistance of the electrolyte can be calculated from Figs. 5a,b, which could be used for *IR*-compensations. In 1.0 M KOH, the resistance of the electrolyte is found to be 5.7–6.8 Ω for the four different samples; while, in 0.5 M H_2SO_4, their resistance is 5.7–7.2 Ω. Furthermore, according to BET results, as shown in Fig. S7, the line of nanobelts display a porous distribution range from 10 to 20 nm (black line), while mesoporous over 30 nm is observed in nanorods (red line). This could explain the difference observed between the as-prepared nanobelts, nanorods and nanoparticles;

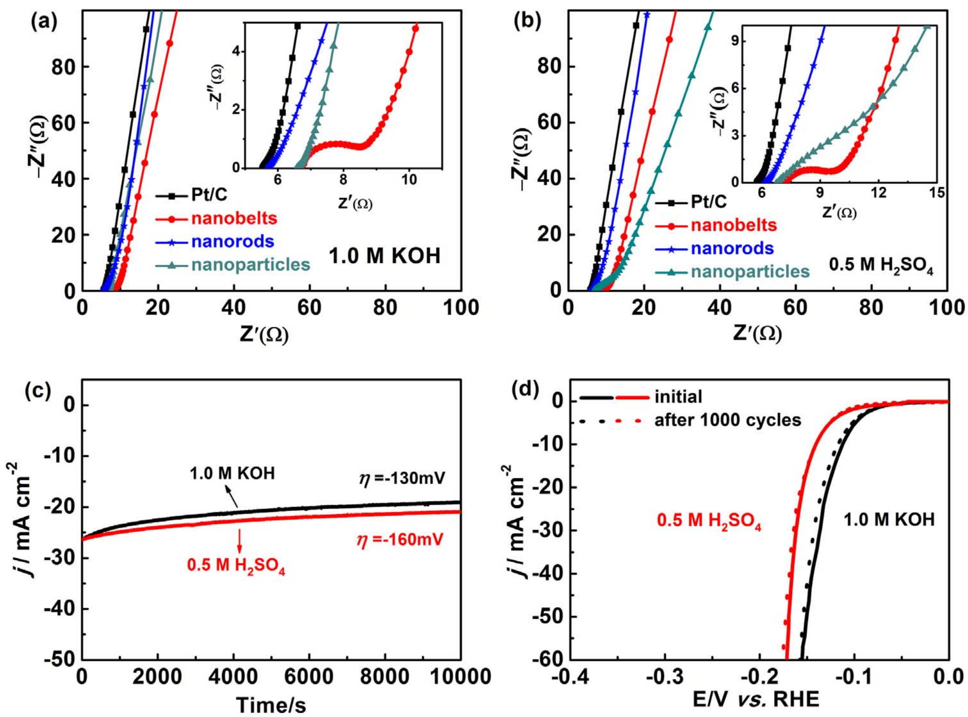

Fig. 5. Nyquist plots in frequency values from 10^5 to 10^2 Hz with a single modulated AC potential of 5 mV in (a) 1.0 M KOH and (b) 0.5 M H_2SO_4 aqueous solution, the insets denote the magnified images of high frequency region. Long-term operation stability of Mo_2C nanobelts, (c) Chronoamperometry curves of Mo_2C nanobelts at $\eta = -160$ mV (0.5 M H_2SO_4) and $\eta = -130$ mV (1.0 M KOH), (d) Polarization curves of Mo_2C nanobelts before and after 1,000 cycles.

these results are consistent with the analysis obtained from SEM.

Meanwhile, as far as we know, long-term stability is one of the most important parameters for HER catalysts, therefore, chronoamperometry curves (time-current curves) and 1,000 cycled-CV curves were also assessed. For this reason, the electrode was operated at $\eta = -130$ mV in 1.0 M KOH and $\eta = -160$ mV in 0.5 M H_2SO_4 to obtain the time-dependent current curves. As shown in Fig. 5c, initially there is a minor current drop, which then gradually stabilizes. After 10,000 seconds of durability tests, a decrease of about 27% in alkaline solutions and 19% in acid is observed. This demonstrates the good stability of Mo_2C nanobelts during the HER process. Besides, a slight drop in current density after 1,000 cycles can be observed in Fig. 5d, which is of about 5 mV in 1.0 M KOH aqueous solution at 10 mA cm^{-2}. While, in 0.5 M H_2SO_4 aqueous solution, the change is even ignorable at 10 mA cm^{-2}, demonstrating the amazing stability both in acidic and alkaline conditions. Notably, the decline in alkaline electrolyte is evidently more serious than that in acid solution, which might be related to the corrosion of carbon [34]. The TEM and EDS mapping images of nanobelts were further collected after 1,000 cycle durability test. As shown in Fig. S8, the morphology of nanobelts didn't change too much after stability test, and the changes of composition and the crystal phase are negligible. The HRTEM image could verify the (101) plane of the hexagonal β-Mo_2C, and the EDS images could confirm the stability of nanobelts after durability test.

Summarizing, such good catalytic performance for hydrogen evolution, observed in this investigation, could be ascribed to the following reasons:

(1) The chain structure (Fig. 1b (ii)) could hinder the aggregation of molybdenum carbides during the high temperature carbonization treatment. The combination between Mo_2C and C could provide a resistance-less path that facilitates electron transfer [34].

(2) The uniform distribution of Mo_2C favors the exposure of active sites, which may enhance the catalytic activity for HER [49,54].

(3) The heteroatom N doped Mo_2C structure could result in the charge density distribution and asymmetry spin, thus enhancing the interaction with H^+ [55,56]. Especially, pyridinic N could enhance the corresponding catalytic performance for hydrogen evolution [43]. Furthermore, the N dopants could possess strong electron-withdrawing features, and make the neighboring C atoms to play dual roles both as electron acceptors and electron donors [32]. Therefore, the uniform structure could reinforce the presence of the synergy between Mo_2C and N dopants, and thus favorable for hydrogen evolution [49].

(4) Nanobelts show higher HER activity than nanorods and nanoparticles, this may root in the unique porous structure that could provide more active sites for water splitting.

4. Conclusions

In this work, an environmentally-friendly and template-free method to prepare Mo_2C in the forms of nanobelts, nanorods and nanoparticles is developed. The introduction of EG, as an intermedium, is significant in forming a circular structure. Water amount and treatment time are also very important during the synthesis procedure, and closely related with the final morphologies of the as-prepared samples. The HER catalytic activity tests display that the Mo_2C nanobelts exhibit an excellent performance for hydrogen evolution, with low onset overpotentials, small Tafel slopes, and excellent cycling stability both in alkaline and acidic solutions. This study might provide a possible cost-efficient and environmental-friendly strategy to design nano-materials with high efficiency for hydrogen evolution.

Acknowledgement

This work was supported by the Fundamental Research Funds for the Central Universities (2015XKMS031), the Natural Science Foundation of Guangxi (2016GXNSFCB380002), the Major International(Regional) Joint Research Project (51210002), the National Basic Research Program of China (2015CB932304), the Natural Science Foundation of Guangdong Province (2015A030312007) and the Guangxi Science and Technology Project (AB16380030). Prof. Tsiakaras is grateful to the Ministry of Educationand Science of the Russian Federation (Mega-Grant, contract no. 14.Z50.31.0001).

Appendix A. Supplementary data

Supplementary data associated with this article can be found, in the online version, at http://dx.doi.org/10.1016/j.apcatb.2017.10.025.

References

[1] X.X. Zou, Y. Zhang, Chem. Soc. Rev. 44 (2015) 5148–5180.
[2] J.J. Lu, L.S. Zhang, S.Y. Jing, L. Luo, S.B. Yin, Int. J. Hydrogen Energy 42 (2017) 5993–5999.
[3] C. Canales, F. Varas-Concha, T.E. Mallouk, G. Ramírez, Appl. Catal. B: Environ. 188 (2016) 169–176.
[4] P.C. Vesborg, B. Seger, I. Chorkendorff, J. Phys. Chem. Lett. 6 (2015) 951–957.
[5] G. Valenti, A. Boni, M. Melchionna, M. Cargnello, L. Nasi, G. Bertoni, R.J. Gorte, M. Marcaccio, S. Rapino, M. Bonchio, Nat. Commun. 7 (2016) 13549.
[6] R.B. Levy, M. Boudart, Science 181 (1973) 547–549.
[7] Z.W. Seh, J. Kibsgaard, C.F. Dickens, I. Chorkendorff, J.K. Nørskov, T.F. Jaramillo, Science 355 (2017) eaad4998.
[8] M. Tavakkoli, N. Holmberg, R. Kronberg, H. Jiang, J. Sainio, E.I. Kauppinen, T. Kallio, K. Laasonen, ACS Catal 7 (2017) 3121–3130.
[9] I. Ledezmayanez, W.D.Z. Wallace, P. Sebastiánpascual, V. Climent, J.M. Feliu, M.T.M. Koper, Nat. Energy 2 (2017) 17031.
[10] D.Y. Chung, S.W. Jun, G. Yoon, H. Kim, J.M. Yoo, K.S. Lee, T. Kim, H. Shin, A.K. Sinha, S.G. Kwon, K. Kang, T. Hyeon, Y.E. Sung, J. Am. Chem.Soc. 139 (2017) 6669–6674.
[11] J. Staszak-Jirkovský, C. Malliakas, P. Lopes, N. Danilovic, S. Kota, K.C. Chang, B. Genorio, D. Strmcnik, V. Stamenkovic, M.G. Kanatzidis, Nat. Mater. 15 (2016) 197–205.
[12] G. Yilmaz, K.M. Yam, C. Zhang, H.J. Fan, G.W. Ho, Adv. Mater. 29 (2017) 1606814.
[13] J.M. Woods, Y. Jung, Y. Xie, W. Liu, Y. Liu, H. Wang, J.J. Cha, ACS Nano 10 (2016) 2004–2009.
[14] D.A. Henckel, O. Lenz, B.M. Cossairt, ACS Catal. 7 (2017) 2815–2820.
[15] Y.J. Ko, J.M. Cho, I. Kim, D.S. Jeong, K.S. Lee, J.K. Park, Y.J. Baik, H.J. Choi, W.S. Lee, Appl. Catal. B: Environ. 203 (2016) 684–691.
[16] A.M. Gómez–Marín, E.A. Ticianelli, Appl. Catal. B: Environ. 209 (2017) 600–610.
[17] G.F. Long, K. Wan, M.Y. Liu, Z.X. Liang, J.H. Piao, P. Tsiakaras, J.Catal 348 (2017) 151–159.
[18] X. Yang, X. Feng, H. Tan, H. Zang, X. Wang, Y. Wang, E. Wang, Y. Li, J. Mater. Chem. A 4 (2016) 3947–3954.
[19] J. Yang, F. Zhang, X. Wang, D. He, G. Wu, Q. Yang, X. Hong, Y. Wu, Y. Li, Angew. Chem. Int. Ed. 55 (2016) 12854–12858.
[20] M. Cabánacevedo, M.L. Stone, J.R. Schmidt, J.G. Thomas, Q. Ding, H.C. Chang, M.L. Tsai, J.H. He, S. Jin, Nat. Mater. 14 (2015) 1245–1251.
[21] Z.H. Pu, S.Y. Wei, Z.B. Chen, S.C. Mu, Appl. Catal. B: Environ. 196 (2016) 193–198.
[22] X.Y. Wang, X. Gan, T. Hu, K. Fujisawa, Y. Lei, Z. Lin, B. Xu, Z.-H. Huang, F.Y. Kang, M. Terrones, R.T. Lv, Adv. Mater. 29 (2017) 1603617.
[23] M. Ledendecker, J. Mondschein, O. Kasian, S. Geiger, D. Göhl, M. Schalenbach, A. Zeradjanin, S. Cherevko, R.E. Schaak, K. Mayrhofer, Angew. Chem. Int. Ed. 129 (2017) 9899–9903.
[24] C.R. Rajamathi, U. Gupta, N. Kumar, H. Yang, Y. Sun, V. Süß, C. Shekhar, M. Schmidt, H. Blumtritt, P. Werner, Adv. Mater. 29 (2017) 1606202.
[25] C. Wan, Y.N. Regmi, B.M. Leonard, Angew. Chem. Int. Ed. 53 (2014) 6407–6410.
[26] Z.Y. Wu, B.C. Hu, P. Wu, H.W. Liang, Z.L. Yu, Y. Lin, Y.R. Zheng, Z.Y. Li, S.H. Yu, Npg Asia Mater. 8 (2016) e288.
[27] B.W. Hao, Y.X. Bao, Y. Le, X.Y. Yu, W.L. Xiong, Nat. Commun. 6 (2015) 6512.
[28] Y. Zhao, K. Kamiya, K. Hashimoto, S. Nakanishi, J. Am Chem.Soc. 137 (2015) 110–113.
[29] S. Reddy, R. Du, L.X. Kang, N.N. Mao, J. Zhang, Appl. Catal. B: Environ. 194 (2016) 16–21.
[30] H.Y. Park, A. Encinas, J.P. Scheifers, Y.M. Zhang, B.P.T. Fokwa, Angew. Chem. Int. Ed. 56 (2017) 5575–5578.
[31] H.X. Ang, H.W. Wang, B. Li, Y. Zong, X.F. Wang, Q.Y. Yan, Small 12 (2016) 2859–2865.
[32] Y. Liu, G. Yu, G.D. Li, Y. Sun, T. Asefa, W. Chen, X. Zou, Angew. Chem. Int. Ed. 54 (2015) 10752–10757.
[33] Y. Liu, G.D. Li, L. Yuan, L. Ge, H. Ding, D. Wang, X. Zou, Nanoscale 7 (2015) 3130–3136.
[34] F.X. Ma, H.B. Wu, B.Y. Xia, C.Y. Xu, X.W. Lou, Angew. Chem. Int. Ed. 54 (2015) 15395–15399.
[35] K. Zhang, Y. Zhao, D. Fu, Y. Chen, J. Mater. Chem. A 3 (2015) 5783–5788.
[36] Y. Huang, Q.F. Gong, X.N. Song, K. Feng, K.Q. Nie, F.P. Zhao, Y.Y. Wang, M. Zeng, J. Zhong, Y.G. Li, ACS Nano 10 (2016) 11337–11343.
[37] H.L. Lin, N. Liu, Z.P. Shi, Y.L. Guo, Y. Tang, Q.S. Gao, Adv. Funct. Mater. 26 (2016) 5590–5598.
[38] Z.D. Yan, N. Gan, D. Wang, Y.T. Cao, M. Chen, T.H. Li, Y.J. Chen, Angew. Chem. Int. Ed. 54 (2015) 14723–14727.
[39] A. Chithambararaj, A.C. Bose, Beilstein J. Nanotech 2 (2011) 585–592.
[40] L. Zheng, Y. Xu, D. Jin, Y. Xie, Chem. Mater. 21 (2009) 5681–5690.
[41] H.L. Lin, Z.P. Shi, S. He, X. Yu, S.N. Wang, Q.S. Gao, Y. Tang, Chem. Sci. 7 (2016) 3399–3405.
[42] M.A.R. Anjum, H.L. Min, J.S. Lee, J. Mater. Chem. A 5 (2017) 13122–13129.
[43] L.F. Lai, J.R. Potts, D. Zhan, L. Wang, C.K. Poh, C. h. Tang, H. Gong, Z. x. Shen, J.Y. Lin, R.S. Ruoff, Energy Environ. Sci. 5 (2012) 7936–7942.
[44] C. Wan, B.M. Leonard, Chem. Mater. 27 (2015) 4281–4288.
[45] Q. Mi, E. Santori, N. Lewis, Chem. Rev. 111 (2010) 5815.
[46] J. Wang, F. Xu, H. Jin, Y. Chen, Y. Wang, Adv. Mater. 29 (2017) 1605838.
[47] J.O.M. Bockris, E.C. Potter, J. Electrochem . Soc. 99 (1952) 169–186.
[48] D. Strmcnik, P.P. Lopes, B. Genorio, V.R. Stamenkovic, N.M. Markovic, Nano Energy 29 (2016) 29–36.
[49] Y.Y. Chen, Y. Zhang, W.J. Jiang, X. Zhang, Z.H. Dai, L.J. Wan, J.S. Hu, ACS Nano 10 (2016) 8851–8860.
[50] L. Huo, B. Liu, G. Zhang, J. Zhang, ACS Appl. Mater. Inter. 8 (2016) 18107–18118.
[51] X. Fan, Y. Liu, Z. Peng, Z. Zhang, H. Zhou, X. Zhang, B.I. Yakobson, X. Guo, R.H. Hauge, ACS Nano 11 (2017) 384–394.
[52] M. Qamar, A. Adam, B. Merzougui, A. Helal, O. Abdulhamid, M.N. Siddiqui, J. Mater. Chem. A 4 (2016) 16225–16232.
[53] P. Xiao, M.A. Sk, L. Thia, X.M. Ge, R.J. Lim, J.Y. Wang, K.H. Lim, X. Wang, Energy Environ Sci 7 (2014) 2624–2629.
[54] H.J. Yan, C.G. Tian, L. Wang, A.P. Wu, M.C. Meng, L. Zhao, H.G. Fu, Angew. Chem. Int. Ed. 54 (2015) 6325–6329.
[55] Y.J. Tang, M.R. Gao, C.H. Liu, S.L. Li, H.L. Jiang, Y.Q. Lan, M. Han, S.H. Yu, Angew. Chem. Int. Ed. 54 (2015) 12928–12932.
[56] J. Duan, S. Chen, M. Jaroniec, S.Z. Qiao, ACS Nano 9 (2015) 931–940.